Finite Element Analysis for Wavelike Flow Marks in Injection Molding

SUNG YONG KANG and WOO IL LEE

Department of Mechanical and Aerospace Engineering
Seoul National University, Seoul 151-742, Korea

Key Words : Flow mark, Injection molding, "Go-Over" hypothesis, Solidified layer

Abstract

The wavelike flow mark phenomenon is one of the surface defects that can arise during the injection stage of the injection molding process. We have performed a numerical analysis using a finite element method for the injection molding to verify the validity of "Go-over" hypothesis. Also, we have compared the results of numerical analysis with available experimental data. Numerical analysis results of the flow marks are qualitatively in good agreement with experimental data of reference, but are quantitatively deviated from experimental data in a consistent manner. A parametric study has been performed to examine the correlative effects of various injection molding processing parameters and material properties on the flow mark size.

Nomenclature

u_i : Velocity
P : Pressure
T_{ij} : Shear stress tensor
d_{ij} : Rate-of-deformation tensor
I_2 : Second invariant of rate-of-deformation tensor
λ_{wave} : Wave-length of flow mark
$\delta(t)$: Thickness of the solidifying layer

1. Introduction

The wavelike flow mark phenomenon is one of the surface defects that can arise during the injection stage of the injection molding process. Wavelike flow marks in injection molding are quite often encountered in different type of polymers, including crystalline as well as amorphous polymer [1-3]. And these defects have been reported at velocities ranging from 1 to 200 mm/s, with wavelengths ranging from 1000 to 10 ㎛ approximately and corresponding depths ranging from 150 to 0.01 ㎛ approximately [1-3].

These surface defects, or wavelike flow marks are generated during filling process in injection molding while polymer melt flows into the cavity (see Fig. 1). Various processing conditions such as injection speed, injection pressure, melt temperature, mold temperature affect these surface defects during the injection stage of process, which eventually determines flow marks wavelength and depth. However, the generation mechanism of this phenomenon is not yet well understood. So far, various generation hypotheses have been suggested such as "Go-over hypothesis", "Buckling hypothesis", "Stick-Slip hypothesis", "Thermal Contraction hypothesis"[1-4].

In this study, we have performed a numerical analysis using a finite element method for the injection molding to verify the validity of "Go-over" hypothesis. Also, we have compared the results of numerical analysis with available experimental data. A parametric study has been performed to examine the correlative effects of various injection molding processing parameters and material properties on the flow mark size.

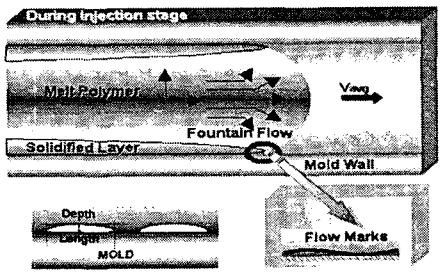

Fig. 1 Schematic diagram of flow domain & shape of flow mark

2. "GO-OVER" HYPOTHESIS

Yoshii et al. [1] suggested this hypothesis, and Yokoi et al. [5] have also supported it. This hypothesis proposes that if cooling against the mold wall takes place very rapidly, a small portion of the flow front surface solidifies, and the still molten polymer above this solidified portion has to "go-over" the solidified melt, creating a gap that takes shape in the valley of the flow mark (see Fig. 2).

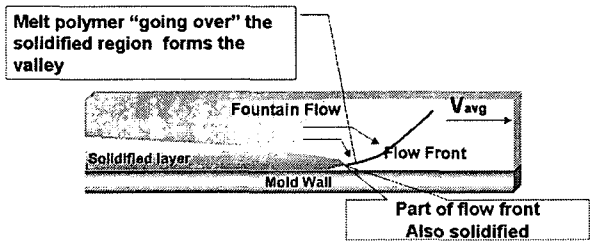

Fig. 2 The "go -over" flow mark generation hypothesis

3. MATHEMATICAL MODELING

3.1 Governing Equations

In present study, we considered the polymer melt flow as two-dimensional because the width of the mold is assumed to be large relative to the thickness. It was assumed that the flow is incompressible quasi-steady.

For the polymer melt flow in the injection molding filling process of thin part geometry, the governing equations such as mass, momentum, and energy conservations can be written as follows according to the Hele-Shaw approximation [6,7].

Continuity:

$$\frac{\partial u_k}{\partial x_k} = 0 \tag{1}$$

Momentum:

$$-\frac{\partial P}{\partial x_i} + \frac{\partial T_{ij}}{\partial x_j} = 0 \tag{2}$$

where u_i, P, T_{ij} are velocity, pressure, shear stress tensor, respectively. Here, all equations are described using the indicial notation and the usual summation convention for repeated indices.

The following Cross-WLF viscosity model is used as a constitutive equation for the shear stress tensor [8,9].

$$T_{ij} = 2\eta(I_2,\theta)d_{ij} \tag{3}$$

$$I_2 = (2d_{ij}d_{ji})^{1/2} \tag{4}$$

$$d_{ij} = \frac{1}{2}\left(\frac{\partial u_i}{\partial x_j} + \frac{\partial u_j}{\partial x_i}\right) \tag{5}$$

$$\eta(I_2,\theta) = \frac{\eta_0(\theta)}{1+(\eta_0(\theta)\cdot I_2/\tau)^{1-n}} \tag{6}$$

$$\theta \geq D_2 \qquad \eta_0 = D_1 e^{-A_1(\theta-D_2)/(A_2+\theta-D_2)}$$

$$\theta < D_2 \qquad \eta_0 = \infty$$

where d_{ij}, I_2, θ are rate-of-deformation tensor, second invariant of rate-of-deformation tensor and temperature, respectively. D_1, D_2, A_1, A_2, τ, n are constant values, varying for different polymers.

Equations (3), (4) are expressed in Cartesian coordinate as follows:

$$T_{xx} = 2\eta(I_2,\theta)\frac{\partial u}{\partial x} \tag{7}$$

$$T_{yy} = 2\eta(I_2,\theta)\frac{\partial v}{\partial y} \tag{8}$$

$$T_{xy} = \eta(I_2,\theta)\left(\frac{\partial u}{\partial y} + \frac{\partial v}{\partial x}\right) \tag{9}$$

$$I_2 = \left[2\left(\frac{\partial u}{\partial x}\right)^2 + 2\left(\frac{\partial v}{\partial y}\right)^2 + \left(\frac{\partial u}{\partial y} + \frac{\partial v}{\partial x}\right)^2\right]^{1/2} \tag{10}$$

Energy :

$$\rho C_p\left(\frac{\partial \theta}{\partial t} + u_j\frac{\partial \theta}{\partial x_j}\right) = \frac{\partial}{\partial x_i}\left(k_{ij}\frac{\partial \theta}{\partial x_j}\right) + \Phi \tag{11}$$

where Φ is viscous dissipation term defined as follows :

$$\Phi = T_{xx}\frac{\partial u}{\partial x} + T_{yy}\frac{\partial v}{\partial y} + T_{xy}\left(\frac{\partial u}{\partial y} + \frac{\partial v}{\partial x}\right)$$

ρ, c_p, k_{ij} are density, specific heat and conductivity of polymer melt respectively.

In order to solve the system of equations (1-6,11) for the field variables, boundary conditions must be given (see Fig.3).

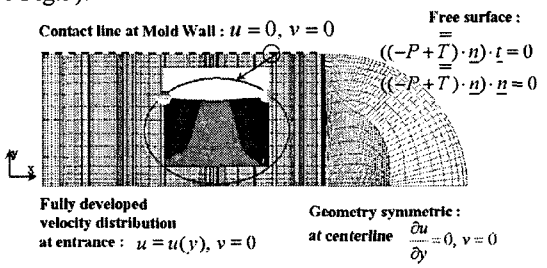

(a) Boundary condition of flow field

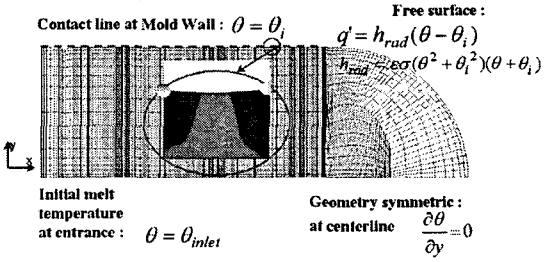

(b) Boundary condition of temperature field

Fig. 3 Boundary Conditions

The centerline of polymer melt is subjected to the symmetric boundary condition. Transverse velocity component is zero and the temperature gradient in the thickness direction is also zero. At the mold wall, the no-slip boundary condition is applied. The velocity components, both normal and tangential to the wall, vanish at the contact point on the wall. Contact resistance may be present at the wall. Therefore the temperature at the mold wall θ_i is given by [13]

$$\theta_i = \frac{\theta_p\sqrt{\rho_p c_p k_p} + \theta_m\sqrt{\rho_m c_m k_m}}{\sqrt{\rho_p c_p k_p} + \sqrt{\rho_m c_m k_m}} \qquad (12)$$

where θ_p and θ_m are the initial temperatures of the polymer and mold, respectively. c_p, k_p, ρ_p and c_m, k_m, ρ_m are the specific heat, conductivity, and density of the polymer and the mold respectively.

The inlet velocity profile at the entrance of the mold is assumed to be that of a steady, fully developed power-law fluid and is given by [6]

$$u = u_{avg}\left(\frac{2n+1}{n+1}\right)\left[1-(1-y)^{1+\frac{1}{n}}\right] \qquad (13)$$

The melt temperature at the entrance to the cavity is assumed to be initial melt temperature θ_p.

As the surface tension is neglected for highly viscous polymer melts, the traction-free boundary condition is imposed on the free surface [11]. Since the density and viscosity of air is much smaller than those of polymer melt, the normal and tangential components of stress can be thought to be negligible, so that

$$(\bar{\bar{\sigma}}\cdot\underline{n})\cdot\underline{t} = 0 \quad (\bar{\bar{\sigma}}\cdot\underline{n})\cdot\underline{n} = 0 \quad \bar{\bar{\sigma}} = -P + \bar{\bar{T}} \qquad (14)$$

where $\underline{n}$ and $\underline{t}$ denote unit normal and tangential vector to the surface. For temperature, the radiation boundary condition between the mold and flow front is imposed on the free surface. The shape factor is 1 because the mold cavity is closed.

$$-k\frac{\partial\theta}{\partial n} = \varepsilon\sigma(\theta^4 - \theta_i^4) = h_{rad}(\theta-\theta_i) \qquad (15)$$

$$h_{rad} = \varepsilon\sigma(\theta^2+\theta_i^2)(\theta+\theta_i)$$

where n, ε, σ are unit normal vector to the surface, emissivity and Stefan-Boltzmann constant, respectively.

4. NUMERICAL SCHEMES

4.1 FEM Formulation of Governing Equations

For finite element analysis, the velocity-pressure formulation is used to solve the continuity and the momentum equations simultaneously. The order of the shape function for pressure is one order lower than for velocity to satisfy the Babuska-Brezzi condition [12]. The bi-quadratic shape function is used for the velocity and the bi-linear shape function for pressure. Rectangular elements are used within the finite element formulation.

Applying the weighted residual method to the continuity and the momentum equations, the Galerkin weighted residual equations are respectively written as

$$< -P_{,x} + T_{xx,x} + T_{yx,y}; w >= 0 \qquad (16)$$

$$< -P_{,y} + T_{xy,x} + T_{yy,y}; w >= 0 \qquad (17)$$

$$< u_{,x} + v_{,y}; q >= 0 \qquad (18)$$

where w and q denote shape functions, ',' represents a spatial derivative, <A;B> is the integration in the domain [9]. We use a frontal elimination technique as a matrix solver and adopt a solution in iterative procedures if relative errors in the previous step are less than 10^{-5} [12].

The generalized form of the boundary condition can be expressed as

E.B.C: $u = \bar{u}, \quad v = \bar{v}$ at $\underline{x} \in \Gamma_E$

N.B.C: $t_x = (-P + T_{xx})\hat{n}_x + T_{yx}\hat{n}_y = \bar{t}_x$ at $\underline{x} \in \Gamma_N$

$t_y = T_{yx}\hat{n}_y + (-P + T_{yy})\hat{n}_y = \bar{t}_y$

After applying the divergence theorem along with the boundary conditions, the governing equations (16-18) become as follows:

$$< -P + T_{xx}; w_{,x} > + < T_{yx}; w_{,y} >= \int_{\Gamma_N} \bar{t}_x w\, d\Gamma \qquad (19)$$

$$< T_{xy}; w_{,x} > + < -P + T_{yy}; w_{,y} >= \int_{\Gamma_N} \bar{t}_y w\, d\Gamma \qquad (20)$$

$$< u_{,x} + v_{,y}; q >= 0 \qquad (21)$$

In order to obtain the finite element formulation, we look for an approximation u, v, and p with shape functions, given respectively by ($w = \tau_i$, $q = \tau_n'$)

$$u = \sum_{j=1}^{M} u_j\tau_j, \quad v = \sum_{j=1}^{M} v_j\tau_j, \quad p = \sum_{n=1}^{N} v_n\tau_n'$$

Using the equation above, the continuity and the momentum equations are summarized in an algebraic form as below

$$A_{ij}u_j - D_{in}P_n + C_{ij}v_j = X_i \qquad (22)$$

$$-D_{jn}u_j - E_{jn}v_j = 0 \qquad (23)$$

$$C_{ji}u_j - E_{in}P_n + B_{ij}v_j = Y_i \qquad (24)$$

where, ($1 \le i, j \le M$, $1 \le n \le N$, M=9, N=4)

$$A_{ij} = < 2\eta(I_2,\theta)\tau_{j,x}; \tau_{i,x} > + < \eta(I_2,\theta)\tau_{j,y}; \tau_{i,y} >$$

$$B_{ij} = < \eta(I_2,\theta)\tau_{j,x}; \tau_{i,x} > + < 2\eta(I_2,\theta)\tau_{j,y}; \tau_{i,y} >$$

$$C_{ij} = < \eta(I_2,\theta)\tau_{j,x}; \tau_{i,y} > \quad D_{in} = < \tau_n'; \tau_{i,x} > \quad E_{in} = < \tau_n'; \tau_{i,y} >$$

$$X_i = \int_{\Gamma_N} \bar{t}_x\tau_i\, d\Gamma \qquad Y_i = \int_{\Gamma_N} \bar{t}_y\tau_i\, d\Gamma$$

We apply the same procedure to energy equation as follows (h is bi-linear shape function, $h = \tau_i$):

$$< \rho c_p \left(\frac{\partial \theta}{\partial t} + u\theta_{,x} + v\theta_{,y} \right) - k\left(\theta_{,xx} + \theta_{,yy}\right) - \Phi; h >= 0 \quad (25)$$

E.B.C: $\theta = \bar{\theta}$ at $\underline{x} \in \Gamma_\theta(t)$

N.B.C: $-k_{ij} \frac{\partial \theta}{\partial x_j} n_i = h_{rad}(\theta - \theta_i)$ at $\underline{x} \in \Gamma_q(t)$

$$< \rho c_p \left(\frac{\partial \theta}{\partial t} + u\theta_{,x} + v\theta_{,y} \right); h > + < k\theta_{,x}; h_{,x} > +$$

$$< k\theta_{,y}; h_{,y} > - < \Phi; h >= \int_{\Gamma_q} k \frac{\partial \theta}{\partial n} h \, d\Gamma \quad (26)$$

Using $\theta(\underline{x}, t) = \sum_{i=1}^{N} \theta_i \tau_i(\underline{x})$, the energy equation is changed into an algebraic form (N=4)

$$M_{ij} \frac{d\theta_j(t)}{dt} + K_{ij}\theta_j(t) = F_i(t) \quad (27)$$

where,

$$M_{ij} =< \rho c_p \tau_i; \tau_j >$$

$$K_{ij} =< \rho c_p (u\tau_{j,x} + v\tau_{j,y}); \tau_i > + < k\tau_{i,x}; \tau_{j,x} > +$$

$$< k\tau_{i,y}; \tau_{j,y} > + \int_{\Gamma_q} h_{rad} \tau_i \tau_j \, d\Gamma$$

$$F_i =< \Phi; \tau_i > + \int_{\Gamma_q} h_{rad} \theta_i \tau_i \, d\Gamma$$

Time is discretized with two-level-β-method [12].

$$\frac{d\Psi}{dt} = f(\Psi) \quad (28)$$

$$\frac{\Psi^{n+1} - \Psi^n}{\Delta t} = \beta f(\Psi^{n+1}) + (1-\beta) f(\Psi^n) \quad 0 \le \beta \le 1$$

Using equations (28), energy equation (27) is written as,

$$\mathrm{M}^{n+\beta} \frac{\theta^{n+1} - \theta^n}{\Delta t} + \beta \cdot \mathrm{K}^{n+1}\theta^{n+1} + (1-\beta) \cdot \mathrm{K}^n \theta^n = \underline{F}^{n+\beta} \quad (29)$$

where

$$\mathrm{M}^{n+\beta} = \mathrm{M}(\theta^{n+\beta}), \quad \underline{F}^{n+\beta} = \underline{F}(t^{n+\beta})$$

$$t^{n+\beta} = \beta \cdot t^{n+1} + (1-\beta) \cdot t^n, \quad \theta^{n+\beta} = \beta\theta^{n+1} + (1-\beta) \cdot \theta^n$$

$$(\mathrm{M}^{n+\beta} + \beta\Delta t \cdot \mathrm{K}^{n+1})\theta^{n+1} = (M^{n+\beta} - (1-\beta)\Delta t \cdot K^n)\theta^n +$$

$$\Delta t \underline{F}^{n+\beta}$$

Due to the non-linearity of the problem, the algebraic equation derived from FEM application, should be solved via an iterative method. Relaxation factor (C_{rf} = 0.7) is introduced to control the convergence speed [9].

For every grid points, the values obtained from the repeated calculation and the values obtained from the previous step are compared to see if they are within the tolerance level of 0.1%.

4.2 Flow Front Advancing Algorithm

Information on the temperature and velocity fields of the previous time step is required to calculate the temperature field of the next step. However, the increment of the calculation region caused by the advance of the flow front makes the process difficult to be obtained.

Generally interpolation is essential because the grid points in the new region do not conform to the grid points of the previous region. Therefore, in order to decide appropriate values for the prior calculation region, the progress of flow front should be slow enough in between time steps, so to speak, giving the time small enough increment, so that the new region does not increase its size too fast. We use the explicit method for the advance of flow front as follows:

$$\underline{x}^{n+1} = \underline{x}^n + \underline{V}\Delta t \quad (30)$$

Grids at the flow front-wall intersection do not move because of the no-slip condition. But there are some cases that new grids formed by flow front advance algorithm pass out of the wall boundary and position themselves outside the wall boundary.

In this case, a straight line connecting the grid points located in and out of the wall and the intersecting points on the wall set to be the new wall-contacting grid points, and reposition the grid points along the flow front (see Fig. 4) [7]. At this point, the time increment should be small enough so that the mass flows through the wall can be ignored.

4.3 Automatic Mesh Generation

The calculation region for numerical analysis would keep changing its shape as the time flows, due to the advancing melt front. This study employs the method of automatic mesh generation during the calculation. An automatic mesh generation routine within the program is assigned for grid reproduction, as well as for the application of the new boundary conditions needed for the reproduced grids.

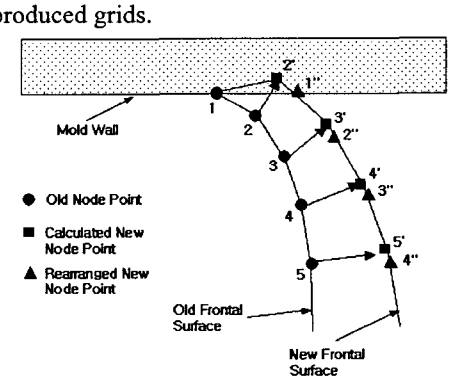

Fig. 4 Flow front advancing scheme

5. PARAMETRIC STUDY

We performed the parametric study in order to find the effects of the processing condition and material properties on suppressing the flow marks.

Concerning the main injection molding parameters that affect flow mark size, there is general agreement that an increase in injection velocity leads to a reduction in flow mark size and the thickness of the layer seems to be proportional to flow mark size [1-5]: the thicker the layer, the longer the flow mark wavelength. We regarded the wavelength as the function of thickness of solidified layer and velocity of flow front as follows:

$$\lambda_{wave} = function(\delta, V_{avg})$$
$$= function(T_s, T_i, \alpha_p, V_{avg})$$

where λ_{wave}, δ, V_{avg}, T_s, T_i, α_p represent the wavelength of flow mark, the thickness of solidified layer, the velocity of flow front, the solidification temperature of polymer, the interface temperature and thermal diffusivity, respectively. By modeling the growth of the solidified layer behind the contact line, we investigated the correlative linkage of the processing conditions and material properties as to affecting flow mark size, and identified whether the simulation works properly.

According to the literatures [13], the following equation for the thickness of the solidifying layer, $\delta(t)$, can be expressed as follows:

$$\delta(t) = \sqrt{2\alpha_p \frac{c_p}{h_{sl}}(T_s - T_w)t} \qquad (31)$$

where T_s, T_w, h_{sl} are the interface temperature between solid phase and liquid phase of the polymer melt, the mold wall temperature and the heat difference between solid phase and liquid phase, respectively.

In Fig. 5, the semi-circles mean the propagation line of the solidified layer beginning with contact line of flow front when flow front comes into contact with the wall of cavity. In order to find when the flow marks generate,

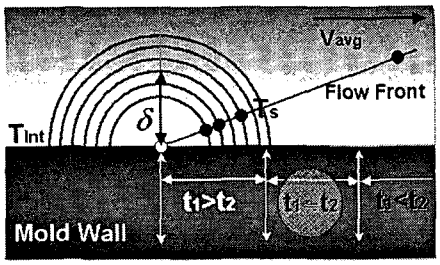

Fig. 5 The propagation of solidified layer

both t_1 that it takes for temperature at certain point of flow front to reach T_s and t_2 that it takes for the point of flow front at the same position as that of t_1 to contact mold wall are introduced for convenience. Very close to the contact line, t_1 is larger than t_2. This means that due to the effect of the fountain flow at the advancing free surface, the flow front near the mold wall comes into the contact with the wall of mold cavity. Far from the contact line of flow front, t_1 is smaller than t_2. That's because the speed of propagation of solidified layer is faster than that of flow front in the direction of thickness.

We assume that the wavelike flow marks generate in such a condition as $t_1 \fallingdotseq t_2$

$$\delta_{t_1=t_2} = \sqrt{2\frac{d_{Distance}}{b_{v-comp}}\frac{c_p}{h_{sl}}(T_s - T_i)\cdot\frac{\alpha_p}{V_{avg}}} \qquad (32)$$

where $d_{Distance}$, $b_{v\text{-}comp}$, V_{avg} are the distance between a point of flow front and mold wall, the velocity fraction of flow front in the direction of thickness and the average velocity of flow front, respectively.

The thickness of solidified layer is considered to be the dominant factor in generation of the wavelike flow marks and be proportional to flow mark size.

$$\lambda_{wave} \propto \delta_{t_1=t_2} = \sqrt{2\frac{d_{Distance}}{b_{v-comp}}\frac{c_p}{h_{sl}}(T_s - T_i)\cdot\frac{\alpha_p}{V_{avg}}} \qquad (33)$$

According to the equation (33), the ways to decrease flow mark size are as follows:

1. A high temperature for the mold, T_m (the effect of T_m on T_i also taken into account)
2. A high flow front velocity, V_{avg}
3. A low value of the polymer solidification temperature, T_s
4. A low value of the thermal diffusivity of the polymer, α_p

These results are in a full agreement with most of the published experimental data in the literatures [1-5].

6. RESULTS AND DISCUSSIONS

We have studied the effects of various processing conditions and material properties on the flow mark size by simulation program. (See Fig.6)

The properties of the polymer material and parameters of the process condition used for the simulation are listed in Table (1-4).

We confirm that proposed formula predicts the effect of various processing conditions and material properties on the flow mark size. In Fig. 7, numerical analysis results of the flow marks are qualitatively in good agreement with experimental data of reference, but are quantitatively deviated from experimental data in a consistent manner.

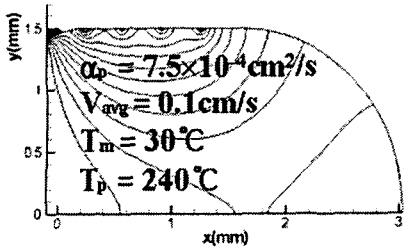

(a) Comparative plot

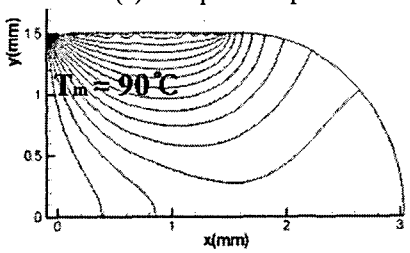

(b) Effect of T_m

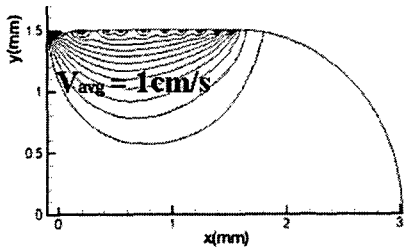

(c) Effect of V_{avg}

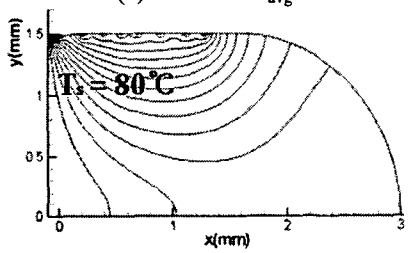

(d) Effect of T_s

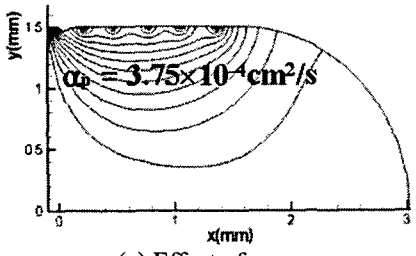

(e) Effect of α_p

Fig. 6. Simulation Results (Temperature Field)

7. Conclusions

The physical modeling and the corresponding numerical analysis system developed in this study will increase our understanding in generation of flow marks and help us establish science-based molding technique for controlling and regulating these surface defects, or flow marks.

Table 1. Density of Polymer and Mold

	Polystyrene (Mitsubishi HT60)	Mold Wall Brass
ρ (kg/m^3)	953.81	8522

Table 2. Specific Heat Dependent on Temperature

T (°C)	90	100	110	120	230	260
c_p(J/(kg °C))	1539	1737	1776	1868	2199	2328

Table 3. Thermal Conductivity Dependent on Temperature

T (°C)	130	161	212	243	264
k (W/(m °C))	0.172	0.192	0.195	0.201	0.211

Table 4. Reference Values of Cross WLF Model

n	τ	A_1	A_2	D_1	D_2
0.3	31250 Pa	25.33	51.6 K	1.2e11 Pas	373.15 K

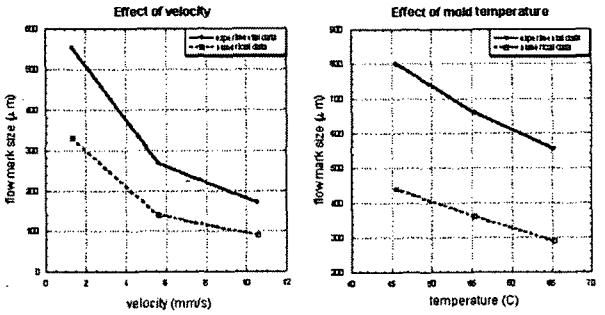

Fig. 7 Comparison of Results by simulation and Experimental Data (Sumitomo E-183)

References

(1) M.Yoshii, H.Kuramoto and K.Kato, Polym.Eng.Sci.,33, 1251 (1993)

(2) T.Yashuhara, K.Kato, N.Otake, and T.Takaiwa, Seikei Kakou (Proc. JSPP Annual Conf., June 6-7, Tokyo), 31 (1995)

(3) L. Tredoux, I. Satoh and Y. Kurosaki, Polym. Eng. Sci., 39, 2233 (1999)

(4) L. Tredoux, I. Satoh, and Y. Kurosaki, Polym. Eng. Sci., 40, 2161(2000)

(5) H. Yokoi, S. Nagami, A. Kawasaki and Y. Murata, SPE ANTEC 94, 368 (1994)

(6) H.S. Lee, Polym. Eng. Sci., 37, 559 (1997)

(7) M.H. Woo and W.I. Lee, M. Eng-Thesis, Seoul National University, Dept. of Mech. Eng. (1996)

(8) M.M. Cross, Journal of Colloid Science, Vol.20, pp.417-437 (1965)

(9) M.J. Crochet, A.R. Davies and K. Walters, Numerical Simulation of Non-Newtonian Flow, Elsevier Science Publishers B.V., Chap9 (1984)

(10) J.N. Reddy, An Introduction to the Finite Element Method, McGraw-Hill Book Co., Chap4 (1984)

(11) J.M. Kim, K.H. Ahn, S.J. Lee, and S.J. Lee, Polym. Eng. Sci., 41, 858 (2001)

(12) C.Taylor and T.G.Hughes, Finite Element Programming of the Navier-Stokes Equations, Pineridge Press (1981)

(13) Arpaci, Vedat S, Poul S. Larsen, Convection Heat Transfer, Englewood Cliffs, NJ: Prentice Hall (1984)